Published by
NIGERIAN SOCIETY OF PHYSICAL SCIENCES
Available online @ https://journal.nsps.org.ng/index.php/jnsps

J. Nig. Soc. Phys. Sci. 8 (2026) 2872

Journal of the Nigerian Society of Physical Sciences

Evaluation of radiation shielding and mechanical properties of palm nut shell ash modernized concrete: a comparative analysis

U. Rilwan[a,*], M. I. Sayyed[b], K. A. Mahmoud[c,d], S. Muhammad[a], A. Alkasim[a], S. I. Ikpughul[a], S. J. Iwa[e], Jibrin Ahmed Guto[f], O. A. Adeyeba[g], M. W. Marashdeh[h]

[a]*Department of Physics, Faculty of Natural and Applied Sciences, Nigerian Army University, P.O.Box 1500, Biu, Borno State, Nigeria*
[b]*Department of Physics, Faculty of Science, Isra University, Amman, Jordan*
[c]*Ural Federal University, St. Mira, 19, 620002, Yekaterinburg, Russia*
[d]*Nuclear Materials Authority, P.O. Box 530, El-Maadi, Cairo, Egypt*
[e]*Department of Physics, Federal University of Technology, Owerri, Imo State, Nigeria*
[f]*Department of Building, Faculty of Environmental, Nigerian Army University, P.O. Box 1500, Biu, Borno State, Nigeria*
[g]*Department of Materials Science and Engineering, King Fahd University of Petroleum and Minerals, Dhahran, 31261, Kingdom of Saudi Arabia*
[h]*Department of Physics, College of Sciences, Imam Mohammad Ibn Saud Islamic University (IMSIU), P.O. Box 90950, Riyadh, 11623, Saudi Arabia*

Abstract

Gamma radiation poses health and environmental risks, creating the need for sustainable, low-cost, and eco-friendly shielding materials. In this study, we modified ordinary concrete with palm nut shell ash (PNSA) to examine its mechanical, physical, and gamma ray shielding performance. The adopted W/C (water-to-cement) ratio was 0.5 for the entire mixtures and the ratio of the samples' masses to their respective volumes gives the densities of our samples. The results reported that, as PNSA advances from 0 to 0.15 kg, the concrete density decreased from 2.40 to 2.25 g/cm^3, accompanied by a rise in porosity from 14.5% to 21.5% as well as an increase in water absorption from 6.8% to 8.6%, 6.4% to 8%, and 5% to 7% respectively for 7, 14, and 28 curing days. The mechanical characteristics decrease as PNSA is added to the concrete matrix. The Monte Carlo N-Particle (MCNP) and Phy-X/PSD simulation results showed that CPNSA2 had superior linear attenuation coefficient (LAC), confirming higher gamma ray attenuation ability. Generally, this work displayed the prospect of adding PNSA for the purpose of shielding against the low and intermediate γ-ray energy. This study contributes by introducing palm nut shell ash as a sustainable cement substitute, demonstrating improved gamma-ray attenuation with CPNSA2, and reducing reliance on costly and toxic conventional shielding materials.

DOI:10.46481/jnsps.2026.2872

Keywords: Gamma radiation shielding, Mechanical properties, Palm nut shell ash, granite, porosity

Article History :
Received: 21 April 2025
Received in revised form: 26 August 2025
Accepted for publication: 25 September 2025
Available online: 19 October 2025

Communicated by: C. A. Onate

1. Introduction

The radiation absorbed dose strictly relied on the decay rate of the radiation source, the exposure period, the released photon energy, the distance between the source and the exposed body and existence of shielding material [1]. The dangerous effects

*Corresponding author Tel. No.: +234-803-777-2627.
Email address: rilwan.usman@naub.edu.ng (U. Rilwan)

of radiation (cancer of breast [2, 3], lung cancer, skin cancer and the rest), even though it can be used for cancer treatments such as liver cancer as reported by Refs. [2, 4], can only be minimized by using efficient materials for shielding in order to achieve the prescribed maximum permissible limit [3, 4].

Several investigations are ongoing on which materials could serve as better additive to concretes in order to safeguard the innocent public from gamma radiation harms [5–10]. Different types and number of materials must be considered to shield different types of ionizing radiation, different source disintegrations and dosages. Although, other factors exist which necessitate other materials for shielding gamma radiation in terms of their heaviness, expensiveness, readily availability in the country, and production process [11, 12].

Mixing cement and other aggregates makes up the concrete composite. The characteristics of concrete like gamma radiation shielding features and mechanical features may be affected by the aggregate type. The varying utilization of concrete in nuclear medicine, nuclear power plants, waste disposal of radioactive materials and linear accelerators, made it a highly acceptable shielding material, and also for its cost effectiveness, ready availability, and environmentally friendly, concrete is most widely used in building applications [13].

In the quest to enhance the gamma radiation attenuation characteristics of a concretes, other researchers introduced hematite to the concrete [14], several studies mixed concretes with ilmenite [15], and various types of concretes were mixed with lime by other researchers [16]. There are other types of concrete were mixed with steel slags [17], and some were mixed with galena [18]. Numerous researchers mixed their concretes with lead [19], part of them with magnetite [20], a fraction of researchers incorporated theirs with limonite [21], other ones with barite [22], varieties of concretes were mixed with waste tire powder as reported by Ref. [23].

Instead of considering local materials as wastes, they could be utilized in concrete production, as cement's partial replacement in order to minimize the utilization of cement or as supplement material to enhance the lifespan and strength of concrete [24], because of its large percentage of SiO_2 and CaO, it can be applied in radiation protection applications [25].

Therefore, this work investigates the impact of partially replacing cement with palm nut shell ash in physical, mechanical and gamma radiation ability of a concrete. MCNP-5 code and Phy-x/PSD were employed to estimate the MAC of the palm nut shell ash incorporated with concrete in different percentages by mass. The study chooses palm nut shell (PNS) because of its availability in the area where the research is carried on and also due to its projected density compared to other local materials found within the area. The study addresses the gap through investigation of the utilization of the cost-effective and readily available PNS as partly replacement of cement in concrete for improved gamma ray shielding.

2. Methodology

2.1. Preparation of the samples

Ordinary concrete was modified in this work by partially replacing cement with palm nut shell ash (PNSA). Four concrete samples were fabricated (one composed of cement, sand (fine aggregate), and granite (coarse aggregate), and the other three composed of cement, sand, granite, and PNSA, with the PNSA replacing the cement in different % by grams). The water-to-cement ratio (W/C) adopted in this work is 0.5. The cement in the concrete was partially replaced by PNSA in percentages of 0 %, 10 %, 20 % and 30 % for samples CPNSA1, CPNSA2, CPNSA3 and CPNSA4 in the same order, respectively. In the fabrication of the control concrete (concrete sample CPNSA1) as in Table 1, 0.5 kg of cement was stirred with 1 kg of sand for 15 minutes before adding the needed quantity of water while stirring for another 15 minutes, then 1 kg of granite was added and the stirring was continued for further 10 minutes to attain homogeneity. For fabrication of the concrete with 10 %, 20 %, and 30 % replacement of cement by PNSA (concrete sample CPNSA2, CPNSA3, and CPNSA4), 0.45 kg, 0.4 kg, and 0.35 kg of cement, 0.05 kg, 0.1 kg, and 0.15 kg of PNSA underwent the same fabrication procedure as CPNSA1. The mixtures obtained were molded with a cylindrical plastic pipe of height (thickness) 6 cm and diameter 2 cm as can be seen in Figure 1. The fabricated cylindrical concrete samples whose densities ranged between 2.25 g/cm^3 to 2.4 g/cm^3 were finally packed and labeled for physical property test (density, porosity and water absorption tests), mechanical property test (compressive strength, flexural strength, and elastic modulus test) and EDXRF analysis to examine the chemical compositions in the samples as presented in Table 2.

The concrete samples' density ([ρ], g/cm^3) is the ratio of the dried samples' mass ([M], grams) to the volume ([V], cm^3). Measurement of the samples' M values utilized digital weighing balance (SF-400) whereas the volume was obtained from the relation given by Ref. [26] in equation (1).

$$V = \pi r^2 h(cm^3), \tag{1}$$

where r and h are the radius and height of the samples respectively. The sample's densities were computed according to Ref. [26] using equation (2).

$$\rho = \frac{m}{V}(g/m^3). \tag{2}$$

The porosity (P, %) of the fabricated samples was gotten by immersing the sample of the concrete in water for period of 48h and the weight was measured and recorded as saturated mass, then the samples were oven-dried at 105 ^{0}C for another 48h, and then re-measured and re-recorded the weight as dried mass. The absorbed water volume (Vp in cm^3) was then calculated according to Ref. [26] via equation (3).

$$V_p(\mathrm{cm}^3) = [\text{mass of saturated samples} - \text{mass of dry samples}] \times \rho_{\text{water}} \tag{3}$$

Figure 1. Procedure for the fabrication of concrete samples.

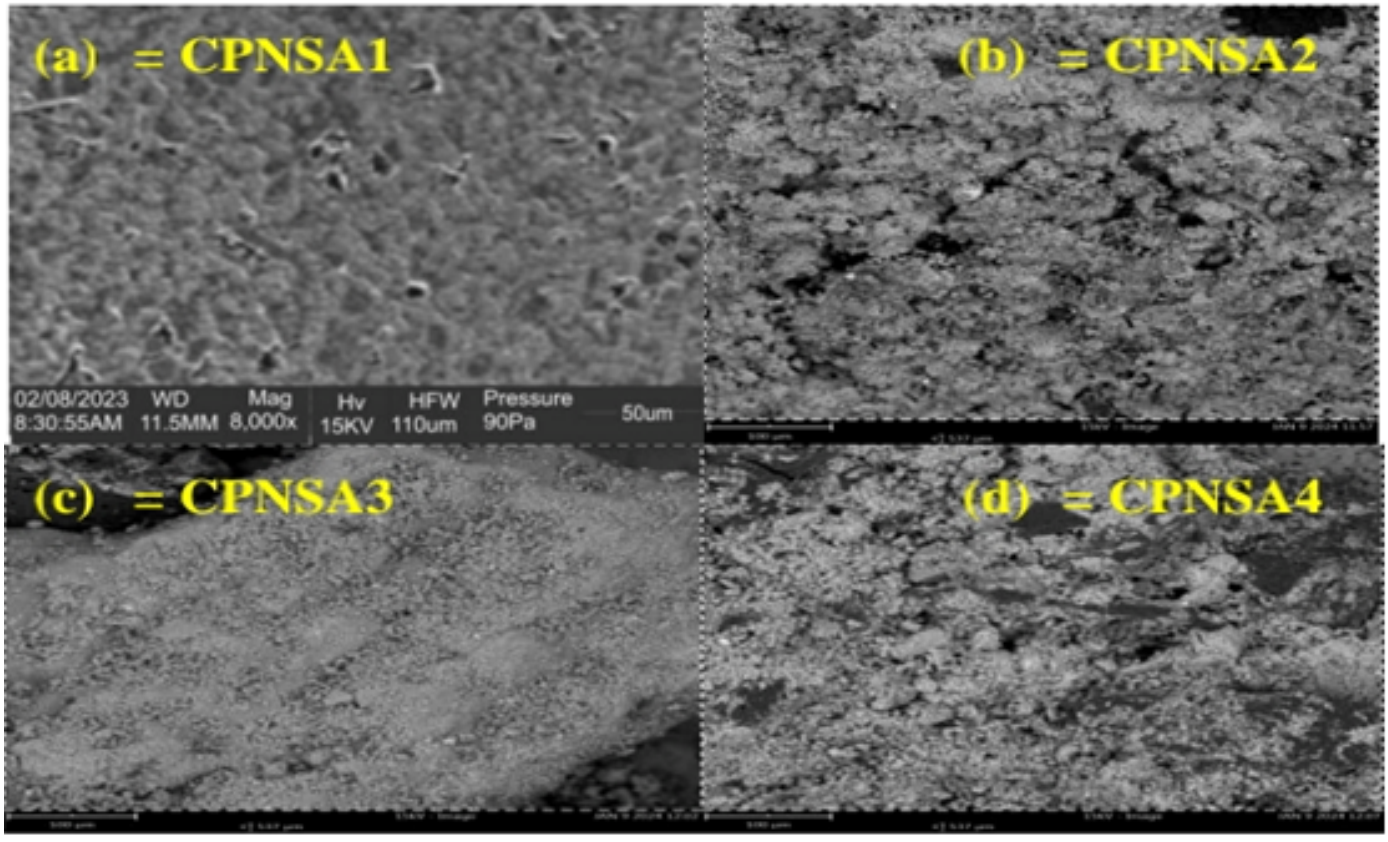

Figure 2. SEM micrographs for the fabricated concretes samples: (a) CPNSA1 (b) CPNSA2 (c) CPNSA3 (d) CPNSA4.

Table 1. Mix proportion of the fabricated concretes.

Sample ID	C (kg)	S (kg)	G (kg)	PNSA (kg)	D (g/cm^3)
CPNSA1	0.50	1	1	0.00	2.40
CPNSA2	0.45	1	1	0.05	2.35
CPNSA3	0.40	1	1	0.10	2.30
CPNSA4	0.35	1	1	0.15	2.25

C = cement; S = sand; G = granite; PNSA = palm nut shell ash; D = density.

Then value P (%) can be determined according to Ref. [27] by equation (4).

$$P(\%) = \left(\frac{V_p}{V} \times 100\right). \quad (4)$$

The capability of withstanding the pressure from all axis is referred to as the comprehensive strength (σc, Kg/cm^2) of the concrete [27]. In another view, it is referred to as the force per unit area required for a concrete to crack [27]. The samples in the form of cylinders were mounted on the load frame. The drive system was adjusted downward in order to mount pressure on the samples. All samples were subjected to loading until they crack at the rate of 0.1 Ns^{-1}. The load cell, applied in series to the sample, gives the applied load which was converted to an electrical signal. The compressive strength (σ_c (MPa)), flexural strength (Fr (MPa)), and elastic modulus (Ec (GPa)) were computed according to Refs. [27–31] by equation (5), (7),

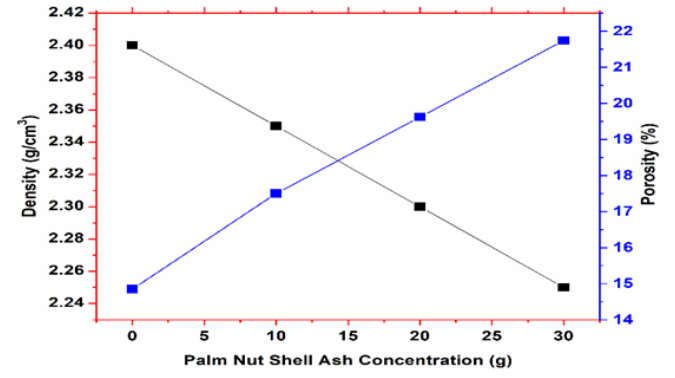

Figure 3. The impact of palm nut shell ash (PNSA) concentration on density and porosity of all fabricated concretes samples (CPNSA1; CPNSA2; CPNSA3; CPNSA4.

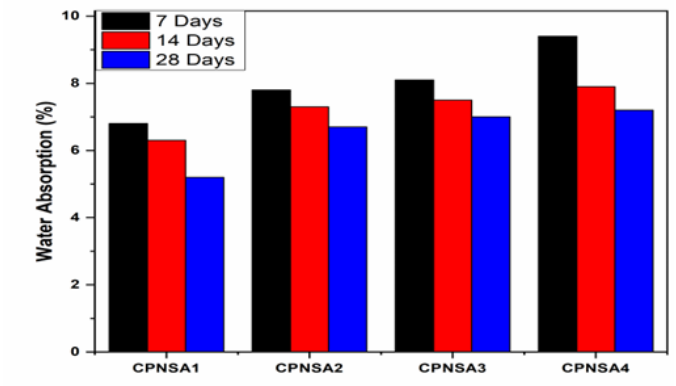

Figure 4. Alteration of water absorption capacity (%) for the fabricated concretes at various curing days.

Table 2. The chemical composition of the fabricated concretes.

Oxides	CPNSA1	CPNSA2	CPNSA3	CPNSA4
CaO	60.84	70.99	67.49	52.84
SiO_2	25.24	10.81	13.55	30.57
Na_2O	0.61	4.23	2.06	1.50
Al_2O_3	2.96	5.70	5.57	4.84
MgO	2.14	2.64	2.66	1.62
K_2O	1.28	1.03	0.61	0.67
Fe_2O_3	2.16	1.20	2.38	2.38
P_2O_5	0.99	1.72	1.95	1.50
SO_3	0.00	1.48	3.41	4.09
TiO_2	0.00	0.20	0.32	0.00
CO_3	3.79	0.00	0.00	0.00

CPNSA = concrete- palm nut shell ash.

and (8).

$$\sigma_c = \frac{P}{A}\left(kg/cm^2\right), \tag{5}$$

where P is the axial load (kg), and A is the concrete's cross-sectional area (cm^2), calculated from according to Ref. [27, 31] in equation (6).

$$A = 2\Pi r\,(r + h), \tag{6}$$

$$F_r(MPa) = 0.7\sqrt{\sigma_c}, \tag{7}$$

$$E_C(MPa) = 5000\sqrt{\sigma_c}. \tag{8}$$

2.2. *Evaluation of the gamma-ray shielding*

The gamma radiation shielding capability (GRSC) parameters of the samples were evaluated using the Monte Carlo N-Particle (MCNP) code and Phy-X/PSD software. The fabricated concretes chemical composition which proved by EDXRF as well as the concretes density were introduced to a previously constructed MCNP input file. The previously generated input file was thoroughly explained in numerous earlier publications [32–35]. The described input file consists of many cards such as surface, cell, importance, material, source, physical, and tally cards. In the source card, the studied gamma-ray energies were extended over a range of 0.015-15 MeV. After that, using equation (9), the simulated ATLs tabulated in the output file were converted to the linear attenuation coefficient ([LAC], cm^{-1} Then, through these simulated values, the HVL (cm), lead's equivalent thickness ([Δ_{eq}], cm), MAC (cm^2/g), radiation protection efficiency ([RPE], %), and transmission factor ([TF], %) were computed using equation (9) - (13) as reported by Ref. [7, 36, 37].

$$\mu\,(\mathrm{cm}^{-1}) = \frac{1}{x}\ln\left(\frac{I_o}{I_t}\right), \tag{9}$$

$$MAC = \frac{\mu(\mathrm{cm}^{-1})}{\rho}\left(\frac{g}{\mathrm{cm}^3}\right), \tag{10}$$

where ρ is the material density in g/cm^3, I_o and I_t are the intensities at time zero and at time t respectively. X is the sample thickness measured in cm, with the MAC in cm^2/g.

Estimation of parameters like the HVL, Δ_{eq} and RPE (%) were via the μ value based on equations (11) - (13) as reported by Ref. [38].

$$\Delta_{0.5}(\mathrm{cm}) = \frac{\ln 2}{\mu}, \tag{11}$$

$$\Delta_{eq}(\mathrm{cm}) = \frac{X(\mathrm{cm})\ln\left(\frac{I_0}{I_t}\right)_{\mathrm{lead}}}{\ln\left(\frac{I_0}{I_t}\right)_{\mathrm{concrete}}}, \tag{12}$$

$$RPE(\%) = \frac{I_a}{I_o} = \left(\frac{I_o - I_t}{I_o}\right)\times 100. \tag{13}$$

3. Results and discussion

As could be seen in Figure 2(a-d), micrographs (scanning electron microscope) normally known as SEM for the entire samples were captured at the ray's energy up to 15 kV. The scaling in μm for the concrete sample CPNSA1 (Figure 2a),

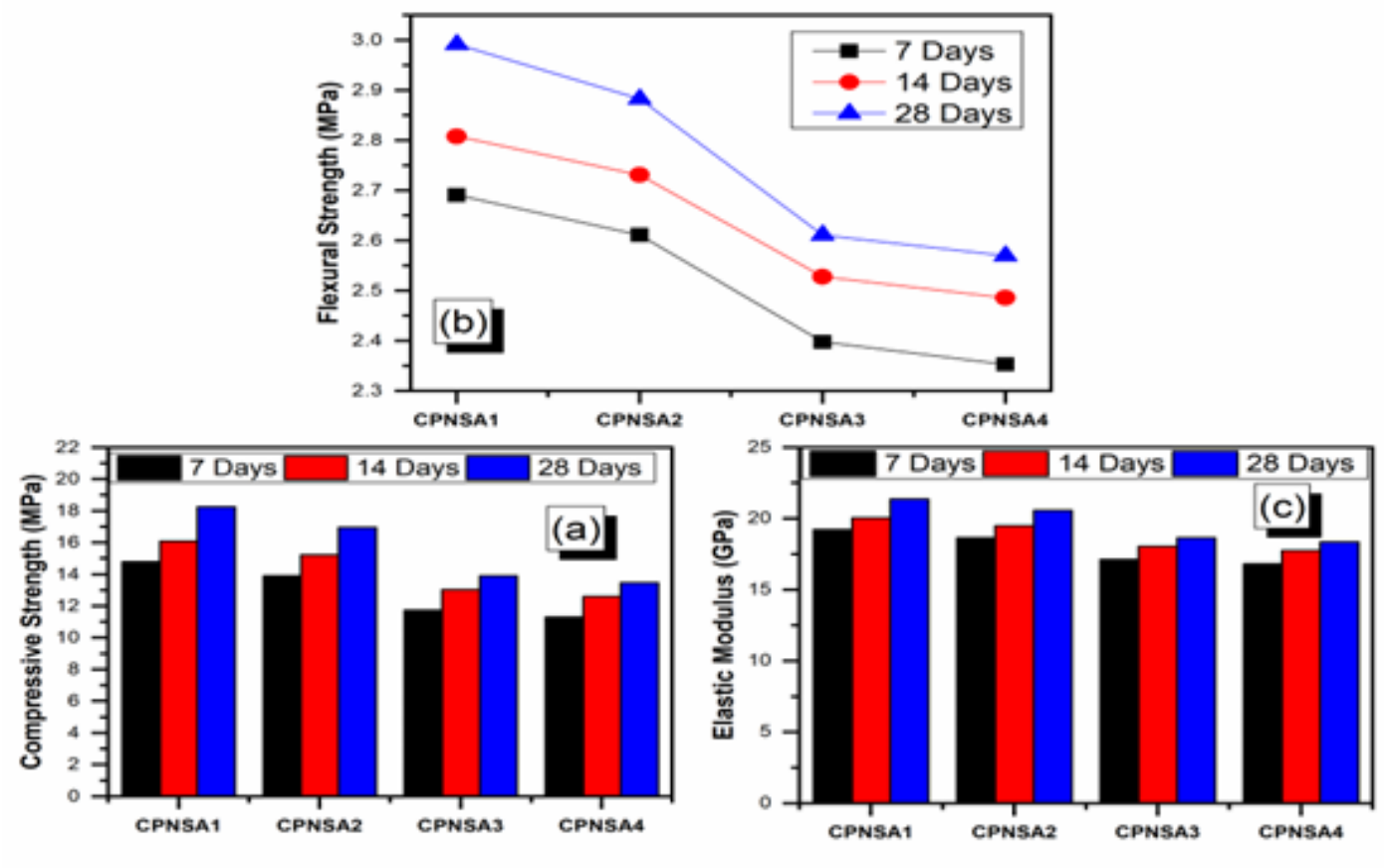

Figure 5. The impact of palm nut shell ash (PNSA) concentration on the fabricated sample's (a) comprehensive strength; (b) flexural strength; (c) elastic modulus.

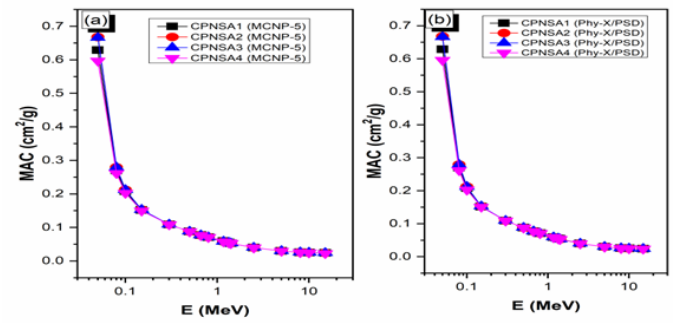

Figure 6. Influence of γ-ray energies on the mass attenuation coefficient (μ_m, cm^2/g) of the fabricated concretes using (a) Monte Carlo N-Particle (MCNP-5) code and (b) Phy-X/PSD program.

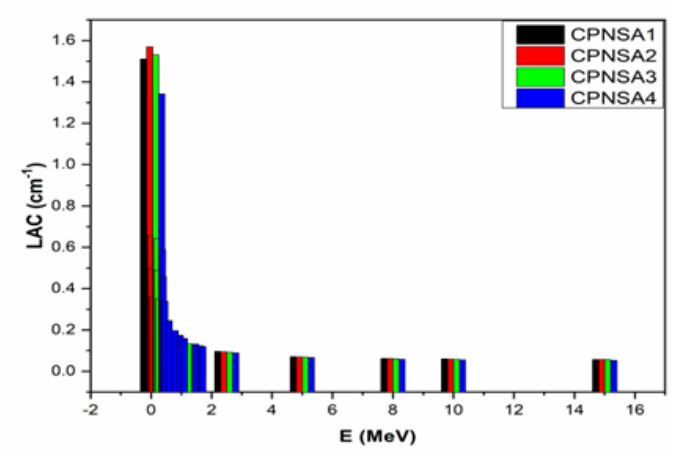

Figure 7. Influence of energies on the linear attenuation coefficient (μ, cm^{-1}) of the fabricated concretes.

CPNSA2 (Figure 2b), CPNSA3 (Figure 2c), and CPNSA4 (Figure 2d) were respectively 50, 100, 100, and 100 μm, where the range of their enlargement was 8 Kx. The results for the micrographs tell that the blended molecules were closely bonded in a denser manner and are throughout distributed within the matrix of the concrete. The produced samples exhibited minimal porosity, which conforms with report of Ref. [5]. In this research work, it was obviously seen that, when the concentration of the reused PNSA is added in the control concrete, the specialty of the partitions of the blended molecules are affected and the molecules become more clustered. This behavior is evidence which confirmed that the addition of the amount of PNSA in the control concrete samples reduces their crystallinity. This behavior was similarly noticed in the work report by Ref. [29].

The analysis of the physical properties (density and porosity) of the investigated concrete samples as shown in Figure 3. It revealed that, as the PNSA content is increasing, the density of

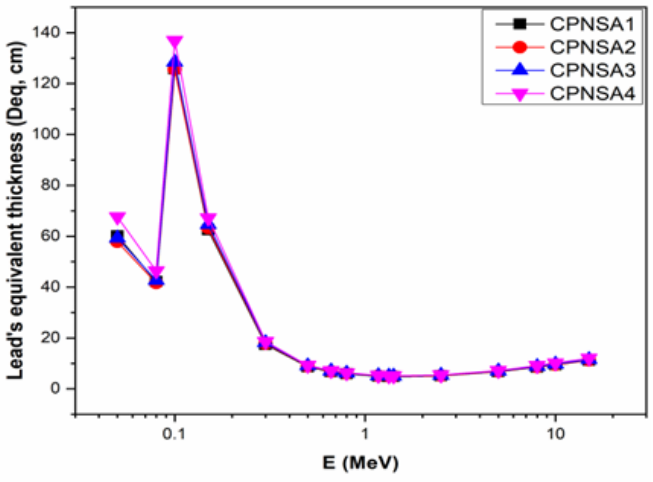

Figure 8. Representation of lead equivalent thickness (Δ_{eq}, cm) against energy.

the samples decreases, while its porosity increases. This trend of increase in porosity when the density decreases is the normal trend for the concrete material, agreeing with the report of Ref. [29]. One of the preferred indicators that tell how durable a concrete will be according to Ref. [29] is water absorption. As such, water absorption in this study was estimated according to the standard set by BS EN 1097-5 in 2008 by using a ventilated oven and a measuring balance. The water absorption after 7, 14 and 28 days of curing for the prepared concrete samples is presented in Figure 4. After 7, 14, and 28 days of curing, the water absorption of the fabricated concretes increases by 44 %, 27 % and 14 %, respectively. For all the samples, the water absorption decreases as the curing days increases. This phenomenon can best be explained by concrete overall voids, since according to Ref. [29], water permits entrance into concrete's voids. The calcium-silicate-hydrate (C-S-H) for the concretes increases and overall voids decreases as the curing period increases. The water absorption of the fabricated concretes is increasing as the content of PNSA is added to the concrete matrix, showing conformity with the report of Ref. [8]. The increasing of water absorption may be attributed to the increase in the overall concrete voids which might have resulted in presence of high carbon particle in the PNSA as reported by Ref. [28].

The results for the mechanical properties such as compressive strength, flexural strength and elastic modulus of the fabricated concretes after 7, 14, and 28 days of wetting curing are depicted in Figure 5a, 5b, and 5c. It was observed that, the compressive and flexural strength as well as elastic modulus increases as the curing days increases from 7, 14 and 28 days. But it decreases as the content of PNSA is added to the concrete matrix for CPNSA2, CPNSA3 and CPNSA4. These results are in line with the result reported by Ref. [28]. The reduced mechanical properties (compressive strength, elastic modulus and flexural strength) can be attributed to the increase in the concentration of CaO in the samples as the content of PNSA is added to the concrete matrix. This result agrees with the report of Ref. [28].

This work succeeded in computing the mass absorption coefficient (MAC) for all the produced concretes samples by utilization of two simulation software (Monte Carlo N-Particle (MCNP-5) and Phy-X/PSD). The results of the comparison between the MAC of the two-simulation software MCNP-5 and Phy-X/PSD for all the prepared concretes are presented in Table 3, where the close agreement, with deviations below ±0.45%, confirms the reliability of both methods and validates CPNSA2's superior γ-ray attenuation capability. As also presented in Figure 6a and 6b, the outcome of the two-simulation software was seen to have a close matching with difference ranging ±1 %. The produced concrete CPNSA2 possessed a superior value of the MAC (0.668 - 0.024 cm^2g^{-1}), then CPNSA3 (0.666 - 0.024 cm^2g^{-1}), after which CPNSA1 (0.629 - 0.024 cm^2g^{-1}) follows, and the last produced sample CPNSA4 (0.597 - 0.023 cm^2g^{-1}) proved to have the least value for MAC within the energy range of 0.05-15 MeV. The reduction in the MAC values with increased γ-photon energy is attributed to the γ-ray interaction modes photoelectric (PE), Compton scattering (CS), and Pair production (PP) which are the main interactions in the low, intermediate, and high energies, respectively. This result is in line with the report published by Refs. [26–29].

Mindfully going through Figure 7, concrete sample CPNSA2 was observed to have possessed a superior value of the LAC (1.570-0.057 cm^{-1}) out of all the produced concrete samples, then CPNSA3 (1.532-0.056 cm^{-1}), thereafter, sample CPNSA1 (1.510-0.057 cm^{-1}) follows, and CPNSA4 (1.342-0.053 cm^{-1}) being the last concrete sample, possessed the smallest value of the linear absorption coefficient (LAC). The reduction in the value of the LAC with the enhanced γ-photon energy is attributed to the same reason discussed previously in the MAC section. This result is in line with the report published by Ref. [30, 34]. As described in Figure 8, the fabricated concretes fatness that possessed a similar protection strength with a unit fatness of ordinary lead at distinct γ-photon-energies. There was a considerable fall in Δ_{eq} within the energy range of .015–0.05 MeV, being the photon electron interaction energy region. Such diminishing could be connected to decrease in the LAC value of Pb (dropping by closely 97 %) as well as the produced samples of concretes (dropping by almost 97 % to 98 %), as the energy advanced from 0.012 to 0.017 MeV. At 0.1 MeV, Δ_{eq} rises as 125.76 cm (CPNSA1), 125.56 cm (CPNSA2), 128.429 cm (CPNSA3), and 136.918 cm (CPNSA4) respectively, which is related to the K-edge possessed by Pb. There was a smooth drop in the lead equivalent values for the prepared concretes between 17.405 cm to 4.78 cm for CPNSA1, 17.759 cm to 4.887 cm for CPNSA2, 18.146 cm to 4.993 cm for CPNSA3, and 18.608 cm to 5.102 cm for CPNSA4 at the intermediate interval of energy as it increases from 0.3 MeV to 1.408 MeV. The steady reductions could be connected to the normal reduction of the values of LAC observed in the produced samples of concretes which reach 60.72% (CPNSA1), 60.88% (CPNSA2), 61.35% (CPNSA3), and 61.42% (CPNSA4) reduction, whereas the diminishing reaches 78% in the case of ordinary Pb. Between 2.5 MeV and 15 MeV, the Δ_{eq} values tend to increase slowly. The increment of Δ_{eq} value could be assigned to advancement in the value of LAC of the produced samples of

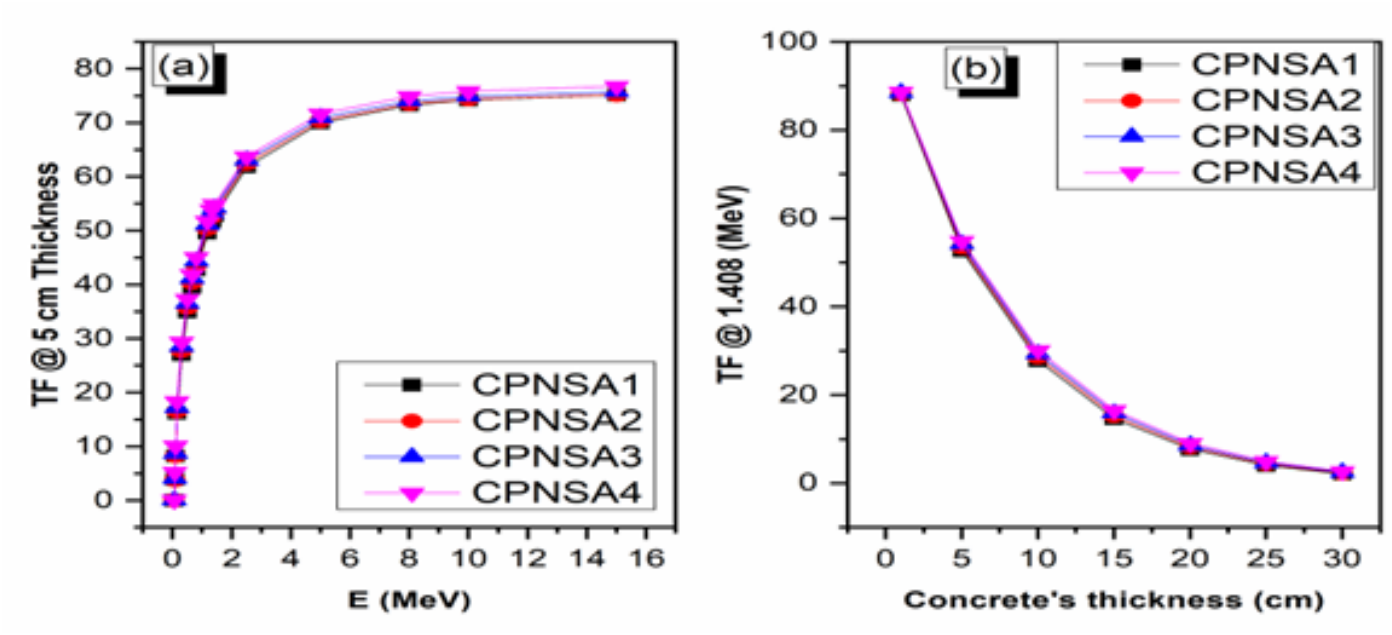

Figure 9. Reliance of transmission factor of the fabricated concretes on (a) γ- energy and (b) concrete's thickness.

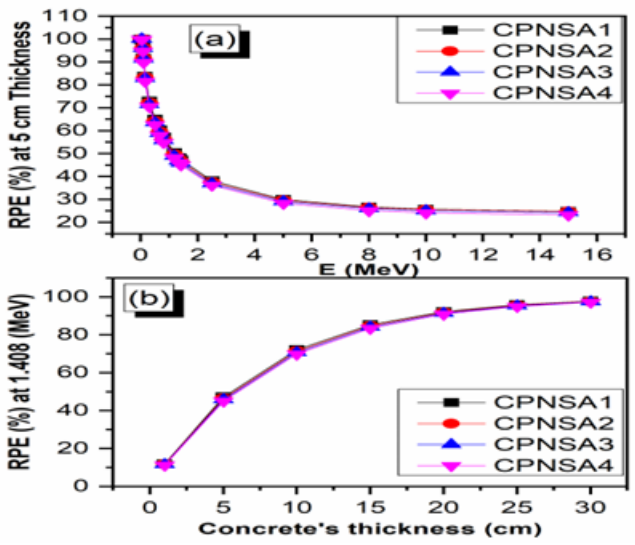

Figure 10. Reliance of radiation protection efficiency of the fabricated concretes on (a) γ- energy and (b) concrete's thickness.

concretes, that advanced by 16.05% (CPNSA1), 17.03% (CPNSA2), 14.66% (CPNSA3), and 13.89% (CPNSA4) from 4.5-15 MeV as the percentage of Pb is improved by 30.2 %. Additionally, the increased concentration of PNSA elevates the Δ_{eq} values through the samples reduced LAC with increased concentration of PNSA. There is a close similarity that existed between the Δ_{eq} result of this study with the results that was published by Refs. [30–37].

Additionally, Figure 9a illustrates how the values of the LAC differs as a function of γ-ray energy and its effects of the transmission factor (TF) values for all the formed samples of concretes. Following the results presented in Figure 9a, the values of the TF was in the order of CPNSA4>CPNSA3>CPNSA1>CPNSA2. The increase of γ-ray energy from 0.05-15 MeV raises the TF for the fabricated concrete samples of 5 cm thickness between 0.05-75.17% (for the CPNSA1), 0.04-75.21% (for the CPNSA2), 0.05-75.73% (for the CPNSA3), and 0.12-76.77% (for the CPNSA4). For the photon or gamma energies smaller compared to 0.05 MeV, the value of the TF that was observed was relatively zero and all the photons energies that were given out from the main sources of the radiation were absorbed with in concrete boundaries. There exists a great similarity between the TF results recorded in this current work and the ones recorded in the work of Refs. [38–45].

In contrary, Figure 9b revealed the calculated TF values against the concrete thickness of all samples at energy of 1.408 MeV. It was obviously seen that, at different thickness, the values of the TF were dropping uniformly, which is due to the path through which the γ-photons follows. within the concrete samples, an increase in the γ-ray path-length enhances the interactions resulted by photon-electrons, which later advances the tendency to which the photons are absorbed. As a result, the TF values reduced between 87.99-2.15% (for the CPNSA1 sample), 88.23-2.34% (for the CPNSA2 sample), 88.47-2.53% (for the CPNSA3 sample), and 88.70-2.74% (for the CPNSA4 sample), increasing the concrete's thickness between 1-30 cm, respectively, agreeing with report of Refs. [28, 46].

Figure 10a and 10b demonstrate the variation of RPE, which reduces as the energy of γ-photon advances for the fabricated concretes versus the concrete's thickness and the energy of γ-photon. The drop in this is because of the fall in the cross-section when the energy of photons advances, confirming prevention of the complete photon absorption by the produced concrete samples. For produced concretes with 5 cm thickness, a

Table 3. Comparison between the Monte Carlo N-Particle (MCNP-5) and Phy-X/PSD mass attenuation coefficient for the prepared concretes at different energies.

Energy (MeV)	Mass attenuation coefficient (cm^2/g)											
	CPNSA1			CPNSA2			CPNSA3			CPNSA4		
	MCNP-5	Phy-X/PSD	Diff (%)	MCNP-5	Phy-X/PSD	Diff (%)	MCNP-5	Phy-X/PSD	Diff (%)	MCNP-5	Phy-X/PSD	Diff (%)
0.015	16.283	16.280	0.019	17.654	17.650	0.023	17.539	17.530	0.049	15.184	15.180	0.028
0.03	2.288	2.287	0.054	2.468	2.467	0.052	2.457	2.455	0.063	2.140	2.139	0.039
0.05	0.629	0.629	0.052	0.668	0.668	0.056	0.666	0.666	0.047	0.597	0.596	0.057
0.08	0.270	0.270	0.039	0.279	0.279	0.069	0.279	0.279	0.042	0.262	0.262	0.053
0.1	0.208	0.208	0.031	0.212	0.212	0.057	0.212	0.212	0.042	0.203	0.203	0.030
0.15	0.152	0.152	-0.061	0.153	0.153	-0.093	0.153	0.153	-0.070	0.150	0.151	-0.086
0.3	0.109	0.109	-0.112	0.109	0.109	-0.113	0.109	0.109	-0.120	0.109	0.109	-0.067
0.5	0.088	0.088	-0.075	0.088	0.088	-0.079	0.088	0.088	-0.077	0.088	0.088	-0.083
0.662	0.077	0.077	-0.121	0.077	0.077	-0.123	0.077	0.077	-0.120	0.077	0.077	-0.118
0.8	0.071	0.071	-0.093	0.071	0.071	-0.086	0.071	0.071	-0.081	0.071	0.071	-0.085
1.173	0.059	0.059	-0.439	0.058	0.059	-0.440	0.058	0.059	-0.450	0.058	0.059	-0.424
1.332	0.055	0.055	-0.372	0.055	0.055	-0.378	0.055	0.055	-0.390	0.055	0.055	-0.373
1.408	0.053	0.054	-0.374	0.053	0.053	-0.393	0.053	0.053	-0.387	0.053	0.053	-0.374
2.5	0.040	0.040	-0.224	0.040	0.040	-0.243	0.040	0.040	-0.229	0.040	0.040	-0.233
5	0.030	0.030	-0.233	0.030	0.030	-0.235	0.030	0.030	-0.229	0.030	0.030	-0.250
8	0.026	0.026	-0.202	0.026	0.026	-0.229	0.026	0.026	-0.216	0.026	0.026	-0.236
10	0.025	0.025	-0.222	0.025	0.025	-0.204	0.025	0.025	-0.233	0.025	0.025	-0.236
15	0.024	0.024	-0.214	0.024	0.024	-0.225	0.024	0.024	-0.198	0.023	0.024	-0.231

CPNSA = concrete- palm nut shell ash.

0.05 to 15 MeV advancement in γ-photon energy resulted in the radiation protection efficiency (RPE) drop by 75.15% (CPNSA1), 75.20% (CPNSA2), 75.72% (CPNSA3), and 76.74% (CPNSA4), aligning with the report of Ref. [29]. Figure 5b depicts the values for the RPE at 1.408 MeV. At this energy, the RPE of the investigated concrete samples were increased with the increase of sample thickness, showing the impact of thickness on the gamma ray attenuation properties. It should be noted, however, that even though at low thickness the values of RPE reported to be significantly lower, some as low as 5 %, compared to higher thicknesses. These values are almost 48.2% and 60.7% at intermediate and higher thickness respectively. Hence, it is vital to consider thickness when assessing the effect of shielding of radiation, especially for space-constraints. The result of this work is in close agreement with the results of Ref. [28, 47].

In Figure 11, we compared the results for the LACs of the prepared concretes with those of previously published concretes at photon energy of 0.662 MeV to facilitate the validation of the presently studied concretes' shielding ability [8, 27–30]. This comparison showed that at 0.662 MeV, samples CPNSA1, CPNSA2, CPNSA3 and CPNSA4 had μ values of 0.185, 0181, 0.178 and 0.174 cm^{-1}, respectively. The above-mentioned values of μ are superior compared to 0% (0.145 cm^{-1}), 10% (0.151 cm^{-1}), 20% (0.150 cm^{-1}), 30% (0.158 cm^{-1}) and 40% (0.161 cm^{-1}) as reported by Ref. [27], EC (0.167 cm^{-1}), B2C (0.175 cm^{-1}), and BC2C (0.178 cm^{-1}) as reported by Ref. [28], M0 (0.0306 cm^{-1}), M1 (0.0479 cm^{-1}), M2 (0.0543 cm^{-1}), M3 (0.0691 cm^{-1}), M4 (0.0757 cm^{-1}), M5 (0.0891 cm^{-1}), M6 (0.1018 cm^{-1}), M7 (0.11306 cm^{-1}) as reported by Ref. [29], and D (0.171 cm^{-1}) as reported by Ref. [8]. On the contrary, the LAC values of the prepared concretes in this work are reported to be lower than that obtained for the concretes S1 (0.1916 cm^{-1}), S2 (0.1909 cm^{-1}), S3 (0.1928 cm^{-1}), S4 (0.1944 cm^{-1}), S5 (0.2065 cm^{-1}) as reported by Ref. [30]. The increased content of Bi_2O_3 which ranged from 20 to 40 wt % in concrete samples S1-S5 may be the reason for the higher μ values in samples S1, S2, S3, S4 and S5, respectively.

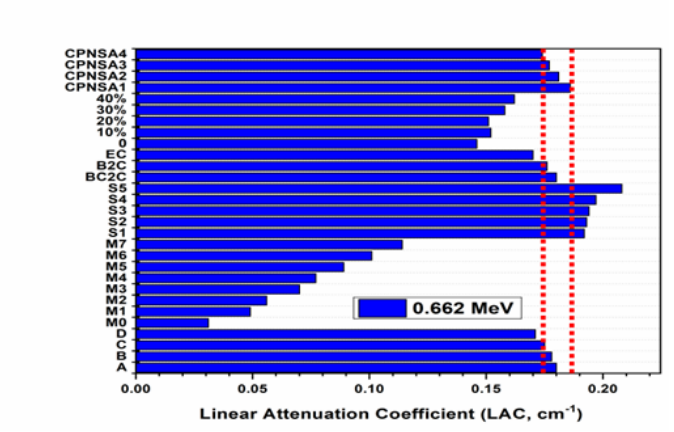

Figure 11. At photon energy of 0.662 MeV, a comparison for the developed concretes' linear attenuation coefficient to that of previously reported concretes.

4. Conclusion

In the current study, ordinary concrete was modified to improve its gamma radiation shielding features through partial replacement of cement by PNSA. The study chooses palm nut shell ash (PNSA) because it is readily available. It is cost-effective, environmentally friendly, and contains a lot of heavy metals such as potassium, calcium and magnesium. Four samples of concretes (CPNSA1, CPNSA2, CPNSA3, and CPNSA4) with different percentages of PNSA substitute was prepared and exposed to considerable testing. The mechanical and physical properties, chemical constituent and gamma ray shielding ability were investigated. The results revealed that, when the content of PNSA is increased, the concrete density is decreased. This was accompanied by a rise in porosity as well as water absorption which could be associated with the concrete's overall voids inside the sample. Even though PNSA is added to the concrete matrix, there is an observable decrease in mechanical properties such as flexural strength, compressive strength and elastic modulus. So, our concrete samples are potentially good for future radiation shielding application. After the computations by Monte Carlo N-Particle (MCNP) code Phy-X/PSD simulation software, it was observed that concrete sample CPNSA2 proved the superior LAC, confirming higher gamma ray attenuation ability. The current study further compares the μ values with previous literatures. The results from this study further emphasized the importance of prioritizing thickness of a material in gamma ray shielding purposes. Generally, this study presented a detailed insight for the optimized performance of concretes, displaying its prospect for the purpose of shielding of gamma radiation.

Data availability

The supporting data for this finding will be available upon reasonable request.

References

[1] N. Zarei, M. R. Rezaie & A. Jomehzadeh, "Radiation hazards investigation of photon scattering by Elekta 6 MeV linac during liver cancer treatment", Chemical Methodologies **6** (2022) 582. https://doi.org/10.22034/chemm.2022.338957.1493.

[2] H. J. Alasali, U. Rilwan, K. A. Mahmoud, T. A. Hanafy & M. I. Sayyed, "Comparative analysis of TiO_2, Fe_2O_3, CaO and CuO in borate-based glasses for gamma ray shielding", Nuclear Engineering and Technology **56** (2024) 4050. https://doi.org/10.1016/j.net.2024.05.006.

[3] C. Thomas, J. Rico, P. Tamayo, F. Ballester, J. Setién & J. A. Polanco, "Effect of elevated temperature on the mechanical properties and microstructure of heavy-weight magnetite concrete with steel fibers", Cement and Concrete Composites **103** (2019) 80. https://doi.org/10.1016/j.cemconcomp.2019.04.029.

[4] U. Rilwan, S. A. Edeh, M. M. Idris, I. I. Fatima, S. F. Olukotun, G. Z. Arinseh, P. Z. Bonat, A. El-Taher, K. A. Mahmoud, T. A. Hanafy & M. I. Sayyed, "Influence of waste glass on the gamma-ray shielding performance of concrete", Annals of Nuclear Energy **210** (2025) 110876. https://doi.org/10.1016/j.anucene.2024.110876.

[5] M. I. Sayyed, A. H. Almuqrin, E. Mohamed & U. Rilwan. "Evaluation of incorporation of granite waste and SnO2-NPs into coating mortar for gamma-ray shielding", Radiation Physics and Chemistry **222** (2024) 111818. https://doi.org/10.1016/j.radphyschem.2024.111818.

[6] S. Bello, J. Simon, A. S. Aliyu, A. Abdulqadir, U. Rilwan & A. El-Taher, "The use of nuclear energy to solve Nigeria's energy crisis and help the country achieve its SDGs", Journal of Radiation and Nuclear Applications **9** (2024) 77. https://www.naturalspublishing.com/Article.asp?ArtcID=28169.

[7] A. H. Almuqrin, M. I. Sayyed, A. Kumar & U. Rilwan, "Characterization of glasses composed of PbO, ZnO, MgO, and B_2O_3 in terms of their structural, optical, and gamma ray shielding properties", Nuclear Engineering and Technology **56** (2024) 2842. https://doi.org/10.1016/j.net.2024.02.047.

[8] U. Rilwan, G. M. Aliyu, S. F. Olukotun, M. M. Idris, A. A. Mundi, S. Bello, I. Umar, A. El-Taher, K. A. Mahmoud & M. I. Sayyed, "Recycling and characterization of bone incorporated with concrete for gamma-radiation shielding applications", Nuclear Engineering and Technology **56** (2024) 2828.https://doi.org/10.1016/j.net.2024.02.045.

[9] M. Ogawa, Y. Nakajima, R. Kubota & Y. Endo, "Two cases of acute lead poisoning due to occupational exposure to lead", Clinical Toxicology **46** (2008) 332. https://doi.org/10.1080/15563650701816448.

[10] U. Rilwan, M. A. Abdulazeez, I. Maina, O. W. Olasoji, A. El-Taher, A. U. Maisalatee, M. U. Sarki, G. Mohammed & M. I. Sayyed, "Feasibility study on the possibility of utilizing e-nut shell ashes for gamma-radiation protection application", Radiation Physics and Chemistry **233** (2025) 112748. https://doi.org/10.1016/j.radphyschem.2025.112748.

[11] U. Rilwan, M. A. Abdulazeez, I. Maina, O. W. Olasoji, A. El-Taher, I. S. Adeshina & M. I. Sayyed, "Sustainable gamma radiation shielding: coconut shell ash modified concrete for radiation protection applications", Journal of Radiation and Nuclear Applications **10** (2025) 33. https://doi.org/10.18576/jrna/100106.

[12] B. Han, L. Zhang & J. Ou, "Radiation shielding concrete. in smart and multifunctional concrete toward sustainable infrastructures", Springer: Singapore **10** (2017) 329. https://link.springer.com/book/10.1007/978-981-10-4349-9.

[13] A. Mesbahi, A. A. Azarpeyvand & A. Shirazi, "Photoneutron production and backscattering in high density concretes used for radiation therapy shielding", Annals of Nuclear Energy **38** (2011) 2752. https://doi.org/10.1016/j.anucene.2011.08.023.

[14] I. M. Nikbin, S. Mehdipour, S. Dezhampanah, R. Mohammadi, R. Mohebbi, H. H. Moghadam & A. Sadrmomtazi, "Effect of high temperature on mechanical and gamma ray shielding properties of concrete containing nano-TiO_2", Radiation Physics and Chemistry **174** (2020) 108967. https://doi.org/10.1016/j.radphyschem.2020.108967.

[15] A. S. Ouda, "Development of high-performance heavy density concrete using different aggregates for gamma-ray shielding", Progress in Nuclear Energy **79** (2015) 48. https://doi.org/10.1016/j.pnucene.2014.11.009.

[16] M. Safajou-Jahankhanemlou & F. Hooriabad-Saboor, "The Influence of Waste Tire Powder on Mechanical and Acoustic Properties of Autoclaved Aerated Concrete", Advanced Journal of Chemistry, Section A **5** (2022) 190. https://doi.org/10.22034/ajca.2022.333553.1306.

[17] M. I. Sayyed, U. Rilwan, K. A. Mahmoud & E. Mohamed, "Experimental study of the radiation shielding characteristics of new PbO-Na_2O-B_2O_3-BaO glasses", Nuclear Engineering and Technology **56** (2024) 2437. https://doi.org/10.1016/j.net.2024.01.058.

[18] A. H. Almuqrin, K. A. Mahmoud, U. Rilwan & M. I. Sayyed, "Influence of various metal oxides (PbO, Fe_2O_3, MgO, and Al_2O_3) on the mechanical properties and γ-ray attenuation performance of zinc barium borate glasses", Nuclear Engineering and Technology **56** (2024) 2711. https://doi.org/10.1016/j.net.2024.02.032.

[19] I. B. Topçu, "Properties of heavyweight concrete produced with barite", Cement and Concrete Research **33** (2003) 815. https://doi.org/10.1016/S0008-8846(02)01063-3.

[20] I. Akkurt & A. M. El-Khayatt, "The effect of barite proportion on neutron and gamma-ray shielding". Annals of Nuclear Energy **51** (2013) 5. https://doi.org/10.1016/j.anucene.2012.08.026.

[21] M. I. Sayyed, H. O. Tekin, O. Kılıcoglu, O. Agar & M. H. M. Zaid, "Shielding features of concrete types containing sepiolite mineral: Comprehensive study on experimental, XCOM and MCNPX results", Results in Physics **11** (2018) 40. https://doi.org/10.1016/j.rinp.2018.08.029.

[22] Y. K. Kaika, I. Umaru, M. M. Idris, U. Rilwan, J. A. Guto, M. I. Sayyed, A. U. Maisalatee, A. A. Mundi & K.A. Mahmoud, "Microstructural, thermal analysis, and gamma-ray shielding properties of bricks made of various local natural materials", Radiation Physics and Chemistry **233** (2025)

112742. https://doi.org/10.1016/j.radphyschem.2025.112742.

[23] A. M. Zeyad, M. A. M. Johari, A. Abutaleb & B. A. Tayeh, "The effect of steam curing regimes on the chloride resistance and pore size of highest strength green concrete". Construction and Building Materials **280** (2021) 122409. https://doi.org/10.1016/j.conbuildmat.2021.122409.

[24] S. A. Yildizel, G. Calis & B. A. Tayeh, "Mechanical and durability properties of ground calcium carbonate-added roller-compacted concrete for pavement", Journal of Materials Research and Technology **9** (2020) 13341. https://doi.org/10.1016/j.jmrt.2020.09.070.

[25] M. M. Idris, I. O. Olarinoye, M. T. Kolo, S. O. Ibrahim, U. Rilwan & M. I. Sayyed, "A comparative study of the radiation dose response of (ZnO)x(TeO2)1-x thin films for high energy X-ray application", Ceramics International **51** (2025) 290. https://doi.org/10.1016/j.ceramint.2025.03.290.

[26] O. M. Ikumapayi, & T. A. Esther, "Composition, characteristics and socioeconomic benefits of palm kernel shell exploitation-an overview", Journal of Environmental Science and Technology **11** (2018) 1. https://doi.org/10.3923/jest.2018.220.232.

[27] M. A. Mydin-Othuman, J. C. Khor & N. Md Sani, "Approaches to construction waste management in Malaysia", In MATEC Web of Conferences, EDP Sciences **17** (2014) 01014. https://doi.org/10.1051/matecconf/20141701014.

[28] R. S. Aita, H. A. Abdel-Ghany, E. M. Ibrahim, M. G. El-Feky, I. E. El-Aassy & K. A. Mahmoud, "Gamma-rays attenuation by mineralized siltstone and dolostone rocks: Monte Carlo simulation, theoretical and experimental evaluations", Radiation Physics and Chemistry **198** (2022) 110281. https://doi.org/10.1016/j.radphyschem.2022.110281.

[29] V. Fugaru, S. Bercea, C. Postolache, S. Manea, A. Moanta, I. Petre, M. Gheorghe, "Gamma ray shielding properties of some concrete materials", Acta Physica Polonica A **127** (2015) 1427. https://doi.org/10.12693/APhysPolA.127.1427.

[30] A. S. Ouda & H. S. Abdelgader, "Assessing the physical, mechanical properties, and γ-ray attenuation of heavy density concrete for radiation shielding purposes", Geosystem Engineering **22** (2019) 72. https://doi.org/10.1080/12269328.2018.1469434.

[31] S. Kumar, K. S. Mann, T. Singh & S. Singh, "Investigations on the gamma-ray shielding performance of green concrete using theoretical, experimental and simulation techniques", Progress in Nuclear Energy **134** (2021) 103654. https://doi.org/10.1016/j.pnucene.2021.103654.

[32] U. Rilwan, M. A. Abdulazeez, I. Maina, O. W. Olasoji, A. El-Taher, I. G. Alhindawi, K. A. Mahmoud, M. I. Sayyed, E. Mohamed, M. Rashad & Y. Maghrbi, "The use of coconut shell ash as partial replacement of cement to improve the thermal properties of concrete and waste management sustainability in Nigeria and Africa, for radiation shielding application", Scientific African **27** (2025) e02578. https://doi.org/10.1016/j.sciaf.2025.e02578.

[33] Aml Almutery, Wan Nordiana Rahman, Faizal Mohamed, Chia Chin Hua, Khairunisak Abdul Razak, Raizulnasuha Ab Rashid, U. Rilwan, M.I. Sayyed, Yasser Maghrbi, "Enhancing the gamma radiation shielding performance: The impact of Bi_2O_3 and MgO nanoparticles on PMMA", Radiation Physics and Chemistry **237** (2025) 113070. https://doi.org/10.1016/j.radphyschem.2025.113070.

[34] M. I. Sayyed, K. A. Mahmoud, S. Biradar, U. Rilwan, L. A. Najam, "Dual-purpose borate-based glasses: optical features and Monte Carlo simulations of gamma radiation shielding", Nuclear Engineering and Technology **57** (2025) 103752. https://doi.org/10.1016/j.net.2025.103752.

[35] U. Rilwan, M. A. Abdulazeez I. Maina O. W. Olasoji S. F. Olukotun, A. El-Taher, M. I. Sayyed, G. Y. N. Chenko, J. A. Guto, O. A. Adeyeba & M. W. Marashdeh, "Gamma Radiation Shielding and Thermal Performance of Concrete with Coconut Shell Ash Replacement", NIPES - Journal of Science and Technology Research **7** (2025) 254. https://doi.org/10.37933/nipes/7.2.2025.27.

[36] K. A. Esraa, M. M. Habiba, M. F. Alrashdi, M. Elsafi, "Studying the shielding ability of different cement mortars against gamma ray sources using waste iron and BaO microparticles, Nexus of Future Materials **1** (2024) 1. https://doi.org/10.70128/583327.

[37] S. Yasmin, M. Saifuddin, S.R. Chakraborty, A.H. Meaze, B.S. Barua, "Evaluation of TeO_2-WO_3-Bi_2O_3 glasses for their potential in radiation shielding with the utilization of the Phy-X software program, Nexus of Future Materials **1** (2024) 51. https://doi.org/10.70128/584048.

[38] Shrikant Biradar, Ashok Dinkar, G.B. Devidas, "A comprehensive study of the effect of bao doping on the physical, mechanical, optical, and radiation shielding properties of borate-based glasses", Nexus of Future Materials **1** (2024) 108. https://doi.org/10.70128/584259.

[39] Zehra Merve Cinan, "Innovative phosphate glasses of advanced material designs for radiation shielding?, Nexus of Future Materials **1** (2024) 92. https://doi.org/10.70128/584052.

[40] K. A Mahmoud, H. M. Alsafi, O. L. Tashlykov, A. M. Abouelsoad, "Investigation of the radiation shielding properties for ZnO and NiO and their based composites, Nexus of Future Materials 1 (2024) 86. https://doi.org/10.70128/584051.

[41] E. L. Ruiz, "Radiation shielding analysis of barium-titanium-borate glasses doped with zinc oxide, Nexus of Future Materials **1** (2024) 80. https://doi.org/10.70128/584050.

[42] V. Setiawan, K. Veeravelan, A. Akouibaa & H. Heryanto, "Comparative half-value layer study of novel PbO-B_2O_3-CuO-CaO glasses versus previous reports", Nexus of Future Materials **1** (2024) 126. https://doi.org/10.70128/585024.

[43] Y. Maghrbi, M. Chouchen & H. B. Rahmouni, "Exploring transmission factor in high-density glasses: the effects of ZnO and Bi_2O_3 concentrations", Nexus of Future Materials **1** (2024) 120. https://doi.org/10.70128/585023.

[44] K. A. Naseer, "Bismuth-doped glasses: a novel approach to efficient radiation attenuation", Nexus of Future Materials **2** (2025) 177. https://doi.org/10.70128/593188.

[45] Kawa M. Kaky, Usama Altimari & Abed Jawad Kadhim, "analytical and comparative study on the impact of CaO on the γ-ray shielding performance of borate-based glasses", Nexus of Future Materials **2** (2025) 172. https://doi.org/10.70128/592452.

[46] P. N. Patil, Manjunatha, M. M. Hosamani, A. S. Bennal & N. M. Badiger, "Influence of PbO_2 and Gd_2O_3 on the gamma-ray shielding performance of borosilicate glasses", Nexus of Future Materials **2** (2025) 210. https://doi.org/10.70128/617892.

[47] Mengge Dong, "From Mineral to high-value shielding material: conversion of ludwigite into polyimide resin-based composites for medical x-rays protection", Nexus of Future Materials **2** (2025) 202. https://doi.org/10.70128/610992.